

## Synthesis and Characterization of ZnO Nanoparticles via Thermal Decomposition for Zn(II) Schiff Base Complex

Hadeer Mohammed Subhi, Ali Taleb Bader\*, and Hazim Yahya Al-Gubury

Department of Chemistry, College of Sciences for Women, University of Babylon, Hilla, Iraq

\* **Corresponding author:**

tel: +964-7710783571

email: wsc.ali.taleb@uobabylon.edu.iq

Received: May 19, 2022

Accepted: July 5, 2022

DOI: 10.22146/ijc.74753

**Abstract:** Zinc(II) oxide (ZnO) nanoparticles were easily produced in this research by thermal decomposition of the Zn(II) Schiff base complex. The ligand was synthesized via condensation of benzylamine with 2-hydroxybenzaldehyde. The Zn(II) Schiff base complex was prepared by the reaction between zinc salt and Schiff base with the molar ratio of 1:1 (metal:ligand). The binary complex powder was calcined at 700 °C to produce ZnO nanoparticles. Various methods were used to characterize the Schiff base, complexes, and nanoparticles, including <sup>1</sup>H and <sup>13</sup>C-NMR, FTIR, TGA, DTA thermal analysis, XRD, TEM, SEM, EDX, BET, UV-Vis Diffuse Reflectance, atomic absorption, melting point, and UV-Vis spectrophotometer. ZnO nanoparticles had an average crystallite size of 48.2 nm.

**Keywords:** Schiff base; Zn(II) Schiff base complex; ZnO nanoparticles

### ■ INTRODUCTION

Schiff bases are compounds that contain the azomethine group (C=N) in their structure and are often formed via the reaction of primary amines and carbonyl groups. Schiff bases are a type of ligand; these ligands, as well as their metal complexes, are important [1-2] because of their capacity to stabilize metal ions in a variety of oxidation states, as well as their use in a variety of catalytic and industrial applications [3]. Because of their unique topologies, structural lability, and sensitivity to molecular environments as a functional material, metal complexes with oxygen and nitrogen donor Schiff bases are of special interest [4]. Zinc complexes of bidentate Schiff-base ligands have recently become popular in several disciplines of research due to their potential uses in biomolecules, catalysts, and optoelectronics [5-6]. There was also a study on the synthesis of numerous salicylaldehydes and benzylamine derivatives Schiff base from simple condensation and their complex [7-10]. Nanoparticles have gotten a lot of interest lately because of their wide range of uses, such as photocatalysis [11]. Zinc(II) oxide is an n-type semiconductor with a 3.37 eV large and direct band gap that can be used in dye-sensitized solar cells [12], gas sensors [13], electric and optical devices [14],

and chemical absorbance [15]. ZnO exists in a range of morphologies, including rod, nanoplate, tube, and its prepared from different methods such as Microwave-assisted thermal methods, electrochemical methods, and sol-gel procedures are all used to make ZnO nanoparticles [16-19]. The thermochemical decomposition of zinc(II) complexes has attracted a lot of interest in recent years [7,11,20-21]. The process of manufacturing ZnO nanoparticles is straightforward, solvent-free, and effective. In this study, the structure of a compound was described using <sup>13</sup>C, <sup>1</sup>H-NMR, FTIR, and UV-Vis. Additionally, ZnO nanoparticles were successfully synthesized using the complex's combustion synthesis approach (Scheme 1). SEM, TEM, XRD, BET, and FT-IR spectroscopy were used to examine the shape and structure of the as-prepared ZnO.

### ■ EXPERIMENTAL SECTION

#### Materials

The salicylaldehyde, benzylamine, absolute ethanol, acetic acid, diethyl ether, and zinc acetate dihydrate (Zn(CH<sub>3</sub>COO)<sub>2</sub>·2H<sub>2</sub>O) were bought (99% purity; Merck company Germany). All compounds were taken without being purified further.

## Instrumentation

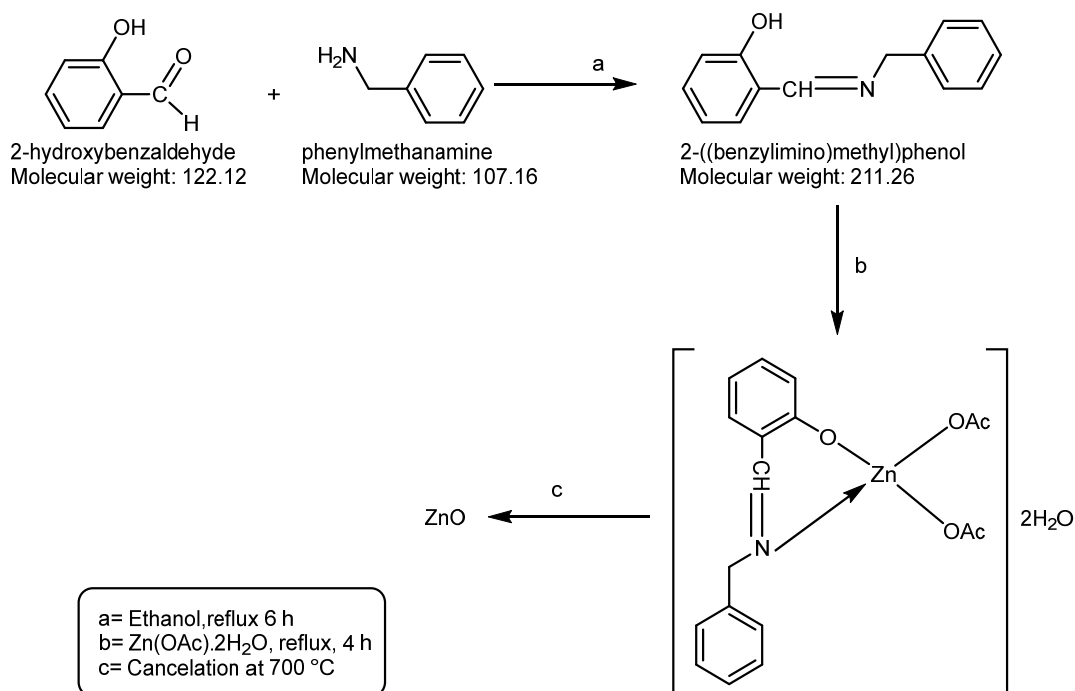
The Fourier-transform infrared spectroscopy (FTIR) measurements of the prepared compounds were performed at  $4000\text{--}400\text{ cm}^{-1}$  using a KBr disc by using an 8400 FT-IR SHIMADZU spectrophotometer. The UV-Vis spectra were measured on (UV-1700) SHIMADZU spectrophotometer in the range of  $300\text{--}800\text{ nm}$ . The UV-visible spectrophotometer with Labspher diffuse reflectance was recorded on the UV-2600 SHIMADZU spectrophotometer (Japan). The thermal analysis for the ligand and complex was conducted by using thermogravimetric analysis (TGA) on DTG-60. The melting point was conducted using Stuart SMP30 (UK). The molar conductivity measurements were obtained using WTW cond 720 (Germany). The cancellation of compounds was done by using furnace Carbolite S336RB (England). The above instruments were obtained at the University of Babylon, College of Science for Women. The produced compounds were measured by nuclear magnetic resonance (NMR) at 400 MHz in  $\text{DMSO-}d_6$  at  $25\text{ }^\circ\text{C}$  and tetramethylsilane (TMS) as the internal standard on a Bruker spectrometer (Germany) in Isfahan

University of Technology (IUT, Iran). The images of ZnO nanoparticles were recorded using a scanning electron microscope (SEM; Zeiss Germany), and a transmission electron microscope (TEM; 912AB, Germany) at the University of Tehran. The X-ray diffractometer (XRD 6000, SHIMADZU, Japan) was conducted in the Ministry of Science and Technology, Baghdad, Iraq. Atomic absorption measurements were obtained by using GBC Avanta Ver 1.33.

## Procedure

### Synthesized of 2-((benzylimino)methyl)phenol ligand

The ligand was prepared by condensation, as shown in Scheme 1. In a 250 mL round bottom flask was placed a mixture of 2-hydroxybenzaldehyde 0.095 mol, 10 mL) and benzylamine (0.095 mmol, 8.93 g) dissolved in 20 mL of ethanol and 2–3 drops of acetic acid with heated to reflux for 6 h. The precipitate obtained was filtered under reduced pressure, dried, and purified by recrystallization from ethanol. The solvent was removed under reduced pressure to yield the ligand as a yellow solid and recrystallization in ethanol m.p. at  $35\text{--}38\text{ }^\circ\text{C}$  [22-23].



**Scheme 1.** Synthesized Schiff base, Zn (Schiff base) complex and of ZnO nanoparticles

The chelation complex, as shown in Scheme 1, was made in a 1:1 (M:L) ratio by adding an ethanolic ligand solution (5.00 g, 0.023 mol) to an aqueous solution of metal salts (5.04 g, 0.023 mol) ( $\text{Zn}(\text{OAc})_2 \cdot 2\text{H}_2\text{O}$ ). For 6 h, the mixture was refluxed at 75 °C and stirred. After cooling to room temperature, a yellow solid precipitant was formed, and the product was filtered, dried, and then recrystallized from hot ethanol m.p. 110–115 °C.

### Synthesis ZnO nanoparticle

ZnO nanoparticles (NPs) were obtained by directly calcining the yellow powders of Zinc Schiff base complex. Approximately 2 g were poured into a platinum crucible, placed in an electrical furnace, and heated at 10 °C/min in the air to 700 °C for 5 h. The ZnO NPs yielded in Scheme 1 were washed in ethanol to remove any remaining contaminants and then dried in the air [24].

## RESULTS AND DISCUSSION

### FTIR Spectra of Schiff Base Ligand

The Schiff base (L) ligand's FTIR spectra in Fig. 1 showed an appearance of a band at 3061  $\text{cm}^{-1}$  due to  $\nu(\text{O-H})$  of the phenol group, proving the existence of a strong intramolecular hydrogen bonding [25]. The synthesis of

Schiff base ligand (L) was confirmed by the assignment of a new stretching vibration band to the  $\nu(\text{C}=\text{N})$  group at 1636  $\text{cm}^{-1}$  [8]. The bands at 2888 and 2842  $\text{cm}^{-1}$  were due to asymmetric and symmetric stretching of  $\nu(\text{CH}_2)$ . Other bands of 3032, 1578, and 1486  $\text{cm}^{-1}$  were due to  $\nu(\text{C-H aromatic})$  st and  $(\text{C}=\text{C})$  st. The FTIR of the Zinc (Schiff base) complex was recorded as KBr discs. The  $\nu(\text{C}=\text{N})$  group at 1636  $\text{cm}^{-1}$  stretching frequency for free ligands (L) was shifted to 1619  $\text{cm}^{-1}$  due to the coordination with the azomethine function to the metal. In the spectra of the complexes, upon metal complexation, the  $\nu(\text{OH})$  phenolic band arising at 3105  $\text{cm}^{-1}$  in the ligand spectrum vanished, and the  $\nu(\text{C-O})$  phenolic underwent a bathochromic shift [8]. The major stretching vibrations of ligands and their complexes are listed in Table 1.

### Nuclear Magnetic Resonance $^1\text{H}$ and $^{13}\text{C}$ -NMR for Schiff Base (2-((Benzylimino)methyl)phenol

The signal assignments for the  $^1\text{H}$ -NMR spectra of Schiff base (ligand L) in  $\text{DMSO}-d_6$  are shown in Fig. 2. The Schiff base proton was detected as a key singlet (s,  $^1\text{H}$ ,  $\text{CH}=\text{N}$ ), 8.2 ppm (1H). The aromatic protons exhibited chemical shifts at 7.2–7.4 ppm (m, 7H, ArH)

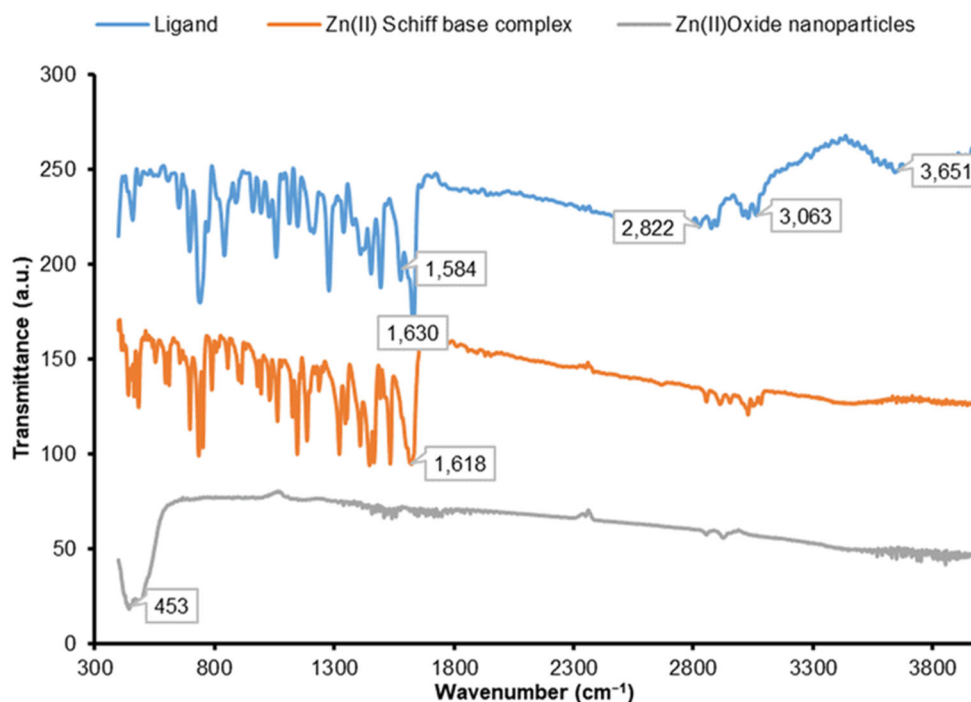
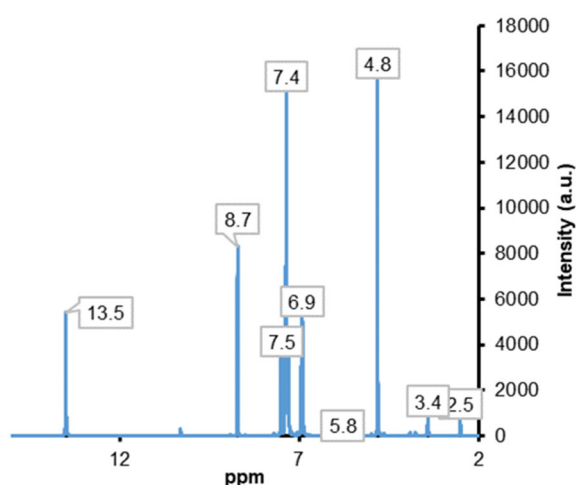


Fig 1. FTIR spectra for Schiff base (ligand), Zn (Schiff base) complex and ZnO nanoparticles

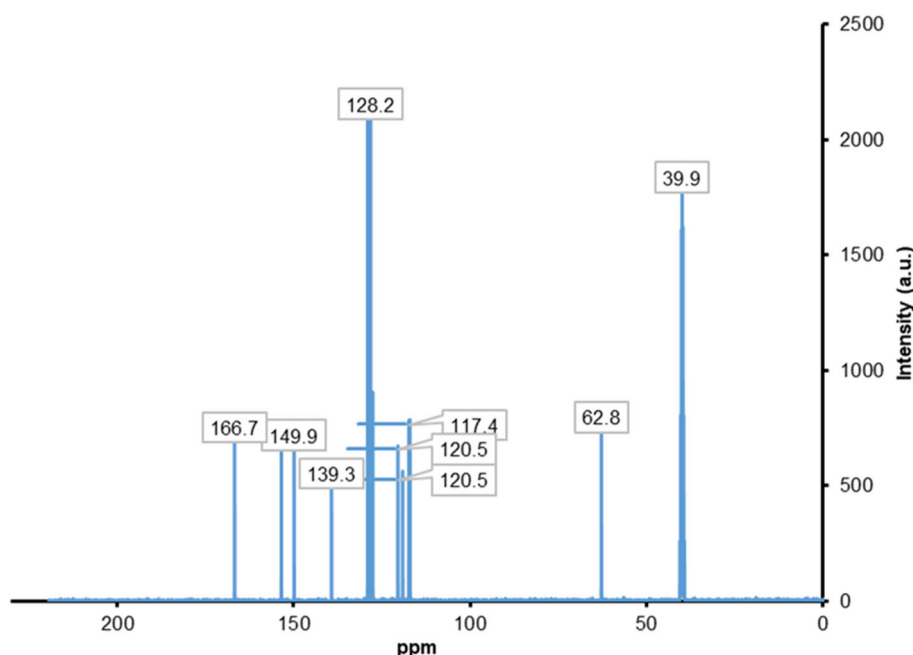
**Table 1.** FTIR data for Schiff base (ligand), Zn (Schiff base) complex, and ZnO

Band	Wavenumber (cm <sup>-1</sup> )		
	Schiff base	Zn (Schiff base)	ZnO
v(O-H)	3061	3105	-
v(C=N)	1636	1619	-
v(CH <sub>2</sub> ) asymmetric and symmetric	2888 and 2842	-	-
-C=C (aromatic)	1578 and 1486	-	-
-C-H (aromatic)	3032	-	-
v(C-O)	1135	1120	-
Zn-O	-	-	474

**Fig 2.** <sup>1</sup>H-NMR spectra for Schiff base (2-((benzylimino)methyl)phenol)

and 6.8–6.9 ppm (m, 1H, ArH). The O-H proton singlet had a significant peak at 13.48 ppm (s, 1H) in the spectra (1H) and the methylene group at 4.5 ppm (s, 2H) [23,25].

The ligand's <sup>13</sup>C-NMR spectra are shown in Fig. 3. A distinguishing feature of the ligand's spectra was the presence of the (N=CH) azomethine group, which appeared at 166 ppm. The carbon of the hydroxyl group was at 153.49 ppm (C-OH). The carbons in aromatic compounds were at 149.88 ppm (C Ar), 139.28 ppm (CH Ar), 129.03 ppm (CH Ar), 128.23 ppm (2C, CH Ar), 127.60 ppm (CH Ar), 120.48 ppm (2C, CH Ar), 119.12 ppm (C Ar), 117.37 ppm (CH Ar), 117.06 ppm (CH Ar) and 62.83 ppm (CH<sub>2</sub>).

**Fig 3.** <sup>13</sup>C-NMR spectra for Schiff base (2-((benzylimino)methyl)phenol)

### Electronic Spectra of Schiff Base (L) and Zinc Complex

The UV-Visible absorption spectra of ligand L in a DMF solution are presented in Fig. 4 and reported in Table 2. The transitions were allocated in two bands at 267 nm,  $37453.18 \text{ cm}^{-1}$  and 316 nm,  $31645.56 \text{ cm}^{-1}$  due to the  $\pi-\pi^*$  and the  $n-\pi^*$  transition. The spectrum of the ZnL complex in DMF solution exhibited three bands at 288 nm,  $34722.20 \text{ cm}^{-1}$ , 300 nm,  $33333.30 \text{ cm}^{-1}$ , and 345 nm,  $28986 \text{ cm}^{-1}$ , which were assigned to  $\pi-\pi^*$  and  $\text{Zn} \rightarrow \text{L}_{\text{CT}}$  transitions in a tetrahedral.

### Thermal Analysis

#### TGA and DTA for Schiff base (ligand) and its Zn(II) complex

Under nitrogen at a rate of  $20 \text{ }^\circ\text{C}/\text{min}$ , Fig. 5 and 6 illustrate TG and DTA trends for the Schiff base (ligand) and its metal ion complexes [26]. The first step, endothermic, is caused by the loss of two adsorbed water

and two acetate molecules as indicated in the temperature of  $30\text{--}323 \text{ }^\circ\text{C}$ . The second endothermic reaction, which is observed in the temperature range of  $323\text{--}490 \text{ }^\circ\text{C}$ , is triggered by the removed of one benzene ring. The third exothermic process, which occurs in the

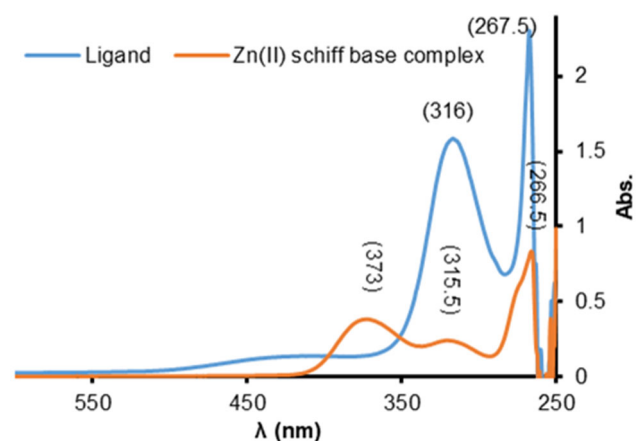


Fig 4. Electronic spectra of Schiff base (L) and zinc complex

Table 2. Electronic spectra of Schiff base (L), zinc complex

Compound	$\lambda_{\text{max}}$ nm ( $\nu \text{ cm}^{-1}$ )	Assignment	Suggested geometry
Schiff base (L)	267 (37453.18), 316 (31645.56)	( $n-\pi^*$ )  ( $\pi-\pi^*$ )	-
ZnL	288, (34722.20) 300, (33333.30) 345, (28986)	( $n-\pi^*$ ) ( $\pi-\pi^*$ ) CTML	Tetrahedral geometry

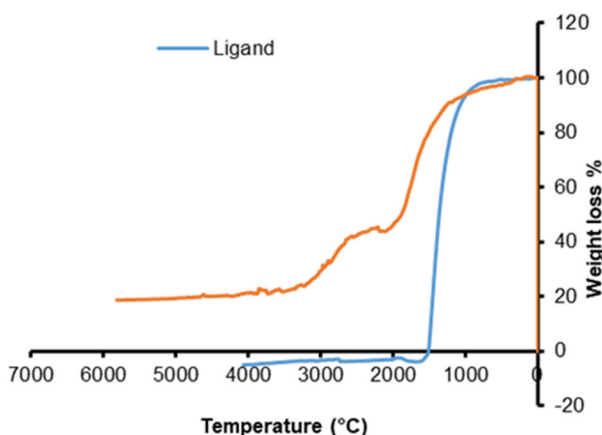


Fig 5. TGA analysis for Schiff base (Ligand) and its zinc complex

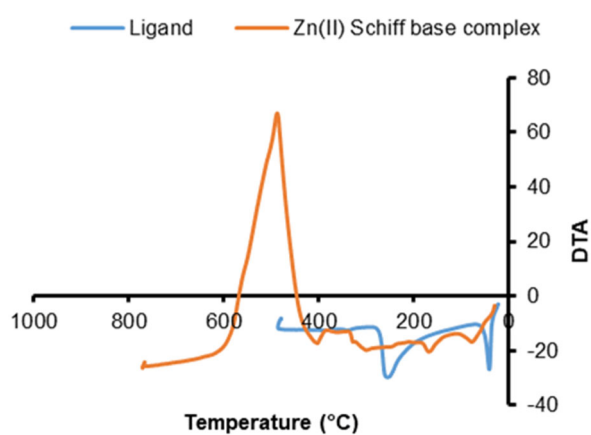


Fig 6. DTA analysis for Schiff base (Ligand) and its zinc complex

temperature range of 490–650 °C, is caused by the breaking up of the organic reduction. Finally, the metal (Zn) oxidized at temperature between 650 and 800 °C, resulting in ZnO [27].

### Characterization of ZnO Nanoparticle

The ZnO NPs were made by calcining a typical complex for 5 h at 700 °C. The nature of the obtained ZnO was validated using FTIR, UV-Vis Diffuse Reflectance, XRD, SEM, TEM, EDX, and BET pattern analysis.

#### FTIR of the ZnO nanostructure

The FTIR pattern of the produced ZnO NPs is shown in Fig. 1 on a scale of 4000 to 400  $\text{cm}^{-1}$ . The absorption bands of ZnO NPs at 474  $\text{cm}^{-1}$  were due to  $\nu(\text{Zn-O})$ . The FTIR spectra obtained clearly showed that ZnO NPs were synthesized [24,28].

#### UV-Vis diffuse reflectance for ZnONps

The Tauc method is a practical and basic approach for measuring a thin film material's characteristic optical band gap [29]. The UV-Vis reflectance spectra of ZnO nanoparticles are shown in Fig. 7. The band gap energy could then be calculated using the Tauc's relation. The UV-Vis reflectance spectrum had a lower scattering effect than absorption. The optical band gap, which corresponded to a sharp reduction in reflectance at a certain wavelength, indicated that the particles in the sample were nearly evenly spread. The direct band gap energy ( $E_g$ ) for ZnO nanoparticles was obtained by fitting the reflection data to the direct transition, as shown in Eq. (1).

$$(\alpha h\nu)^{\gamma} = A(h\nu - E_g) \quad (1)$$

where  $\alpha$  is the absorption coefficient,  $h\nu$  is the photon energy, and  $E_g$  is the direct band gap. The direct band gap was 3.2 eV when plotting  $(h\nu)^2$  as a function of photon energy and projecting the linear component of the curve to absorption equal to zero [30-31].

#### X-Ray diffraction (XRD) analysis for the ZnO nanoparticles

The X-Ray beam incident on a sample and diffracted by the crystalline phases based on Bragg's law, as shown by Eq. (2), is the fundamental approach used to estimate the solid crystalline structures and crystallite size [32].

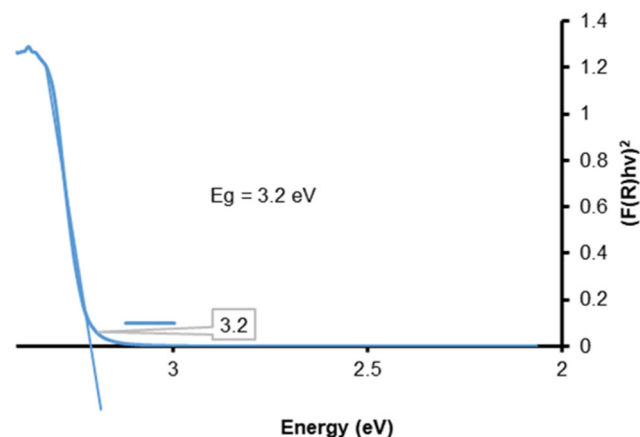


Fig 7. Energy band gap for ZnO Nps

$$n\lambda = 2d \sin \theta \quad (2)$$

where  $n$  is the order of reflection,  $\lambda$  is the wavelength of X-Rays, and  $\theta$  is the Bragg angle. Then,  $d$  spacing was calculated, allowing for easy identification of material structure in the interplanar spacing. The shape, position, and intensity of the peak are the most important aspects of a diffraction pattern. The structure of the investigated material can be modulated after assigning Miller indices ( $h,k,l$ ) to each unit cell and comparing peak positions to standard patterns published by the International Center for Diffraction Data (ICDD). Sherrer's formula Eq. (3) can also be applied to the XRD data to determine the crystallite size [33].

$$L(D) = \frac{K\lambda}{B \cdot \cos \theta} \quad (3)$$

where  $L$  or  $(D)$  is the crystal size,  $K$  (0.94) is a constant that depends on the crystal type,  $\lambda$  (1.54180 Å) is the wavelength of X-Ray,  $B$  is FWHM (full width at half maximum), and  $\theta$  is Bragg's angle [34].

Fig. 8 compares the X-Ray diffraction data of ZnO NPs to the JCPDS 01-076-0205 standard reference for ZnO. Diffraction peaks (100), (002), (101), (102), (110), (103), and (112) were found and were confirmed by the hexagonal ZnO (Wurtzite) according to the standard reference. Through the figure, three very clear zinc oxide peaks were noted at the angles 31.96°, 34.84°, and 36.42° compared to the JCPDS card.

#### SEM for synthesized ZnO

The morphology of ZnO nanoparticles sintered at 700 °C in Fig. 9 was studied using SEM techniques to

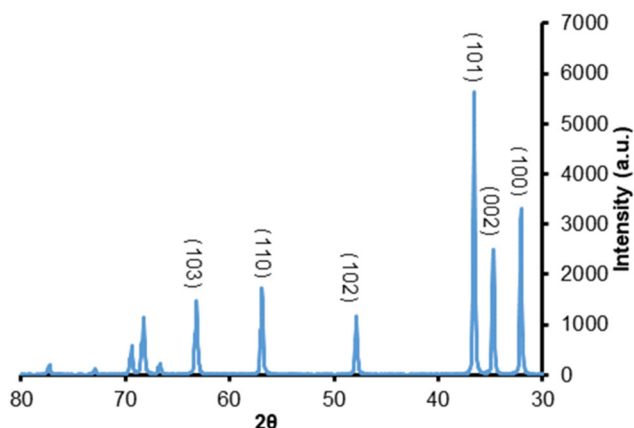


Fig 8. XRD for ZnO nanoparticles

collect useful information about the structure of the produced nanoparticles. Gaussian and SEM picture

micrograph investigations showed irregular aggregated distribution and aspherical shape. According to the histogram, the average grain size was between 40 and 190 nanometers.

#### EDX analysis of ZnO nanoparticles

The production of ZnO NPs was studied using EDX analysis. Various locations were concentrated during the EDX measurement. The relevant peaks are shown in Fig. 10. The EDX spectrum revealed the presence of ZnO in the produced nanostructure. The atomic percent values of Zn and O in the spectrum were 86.7 and 13.3, respectively. In the synthesized samples, there was a presence of Zn and O dopants. There was no significant quantity of impurities found.

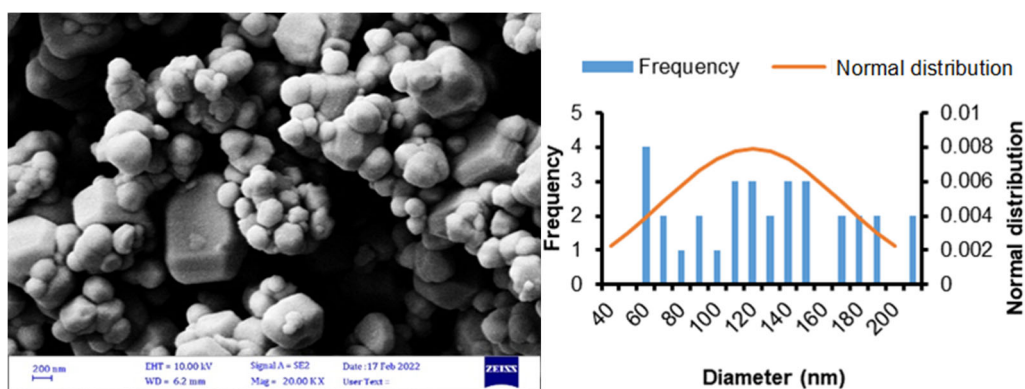


Fig 9. SEM and Histogram for ZnO nanoparticles

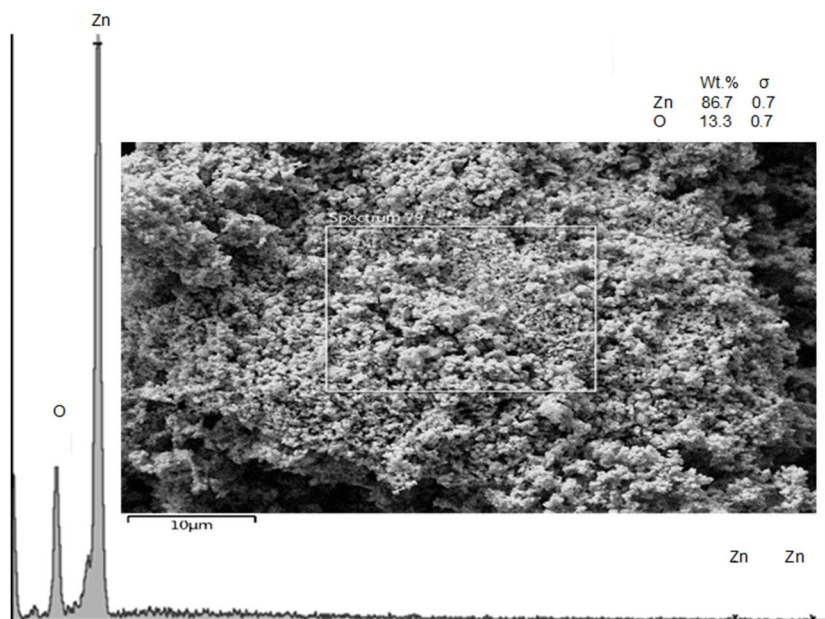


Fig 10. EDX analysis for ZnO nanoparticles

### TEM of ZnO nanoparticles

Fig. 11 shows the TEM images of ZnO. The TEM investigation was held to better understand the nanoparticles' crystalline properties and size. The TEM images of ZnO showed that the particles were virtually hexagonal with a minor thickness variation, confirming the SEM findings [35]. Fig. 11 shows that TEM morphology surface analysis is used to analyze the morphology of the surface of ZnO nanoparticles.

### Surface area analyzer

The nitrogen isothermal adsorption technique shown in Fig. 12 was used to determine the surface area and pore structure of the ZnO nanoparticles. The isotherm profiles of ZnO showed a minor hysteresis loop, which could be classified as type IV. The surface area, average pore diameter, and total pore volume for ZnO are listed in Table 3. The high surface energy of ZnO nanoparticles is thought to be the source of nanoparticle aggregation or the creation of bigger nanoparticles [36]. From the nitrogen adsorption/desorption studies, the BET



Fig 11. Transmittance electron microscopy for ZnO NPs

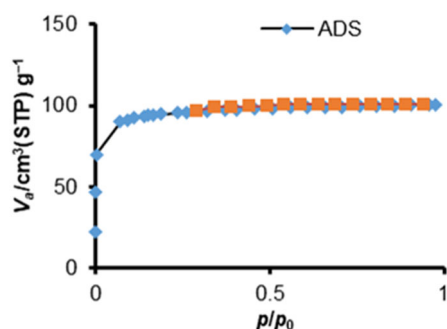


Fig 12. Nitrogen adsorption-desorption isotherms for ZnO NPs

Table 3. Surface physical characteristics of ZnO

Surface physical parameters	Value
Surface area	363.61 [m <sup>2</sup> g <sup>-1</sup> ]
Average pore diameter	83.54 [cm <sup>3</sup> (STP) g <sup>-1</sup> ]
Total pore volume	0.1558 [cm <sup>3</sup> g <sup>-1</sup> ]

method was utilized to compute the  $S_{\text{BET}}$  of ZnO nanoparticles. Prior to analysis, the material was degassed for two hours at 100 °C. The following equation was used to determine the diameter of ZnO nanoparticles:

$$d_{\text{BET}} = \frac{6000}{\rho_{\text{sample}} * S_{\text{BET}}} \quad (4)$$

where the sample is the density of ZnO powder (5.60 g/cm<sup>3</sup>),  $S_{\text{BET}}$  is the BET-specific surface area (m<sup>2</sup>/g), and  $d_{\text{BET}}$  is the mean crystalline size (nm).  $d_{\text{BET}}$  Values of 5.72 nm for ZnO nanoparticles annealed at 700 °C were found using Eq. (4). The difference between the XRD Scherrer formula and the BET methods for determining the mean crystalline size of ZnO nanoparticles suggested that there were agglomerations in the ZnO nanoparticles.

### CONCLUSION

Salicylaldehyde, phenylmethanamine, and zinc acetate were used to create a binary Zn Schiff-base complex. FTIR, <sup>1</sup>H-NMR, <sup>13</sup>C-NMR, TGA, DTA, and UV-Vis were utilized to determine the structure of the new Zn(II) complex produced and describe the formation of Schiff base ligand and metal with a molar ratio of 1:1. These observations led to the suggestion of deformed tetrahedral molecular geometries for the metal complex. Thermal decomposition was employed to make ZnO NPs with a 3.2 eV bandgap energy and particle sizes of 48 nm. The results of XRD, EDX, SEM, TEM, and BET revealed that single-phase ZnO NPs with particle sizes of less than 100 nm were produced via solid-state thermochemical decomposition of binary Zn-Schiff base complex. These findings might be utilized to predict the behavior of ZnO NPs, to serve as a foundation for future research at the *in vitro* and *in vivo* levels of experiments, and in the photodegradation of dye.

## ■ REFERENCES

- [1] Mahmoud, W.H., Omar, M.M., Sayed, F.N., and Mohamed, G.G., 2018, Synthesis, characterization, spectroscopic and theoretical studies of transition metal complexes of new nano Schiff base derived from L-histidine and 2-acetylferrocene and evaluation of biological and anticancer activities, *Appl. Organomet. Chem.*, 32 (7), e4386.
- [2] Sahin, M., Kocak, N., Arslan, U., Sahin, O., and Yilmaz, M., 2013, Bis-Schiff base derivatives of 2,5-dihydroxybenzaldehyde: Synthesis, characterization and antimicrobial activity of their Cu(II), Co(II) and Zn(II) complexes, *J. Macromol. Sci., Part A: Pure Appl. Chem.*, 50 (8), 821–827.
- [3] El-Sonbati, A., Mahmoud, W., Mohamed, G.G., Diab, M., Morgan, S.M., and Abbas, S.Y., 2019, Synthesis, characterization of Schiff base metal complexes and their biological investigation, *Appl. Organomet. Chem.*, 33 (9), e5048.
- [4] Dey, D., Kaur, G., Patra, M., Choudhury, A.R., Kole, N., and Biswas, B., 2014, A perfectly linear trinuclear zinc–Schiff base complex: Synthesis, luminescence property and photocatalytic activity of zinc oxide nanoparticle, *Inorg. Chim. Acta*, 421, 335–341.
- [5] Turk, P., Singh, K., and Dhanda, A., 2022, Synthesis, spectroscopic, electrochemical, thermal and antimicrobial studies of Ni(II), Zn(II), Cu(II) and Co(II) metal complexes of novel bidentate Schiff base ligand, *J. Iran. Chem. Soc.*, 19 (9), 3797–3813.
- [6] Saeednia, S., Iranmanesh, P., Ardakani, M.H., Mohammadi, M., and Norouzi, G., 2016, Phenoxo bridged dinuclear Zn(II) Schiff base complex as new precursor for preparation zinc oxide nanoparticles: Synthesis, characterization, crystal structures and photoluminescence studies, *Mater. Res. Bull.*, 78, 1–10.
- [7] Gharagozlou, M., Naghibi, S., and Ataei, M., 2018, Water-based synthesis of ZnO nanoparticles via decomposition of a ternary zinc complex containing Schiff-base, chelating, and Phen ligands, *J. Chin. Chem. Soc.*, 65 (10), 1210–1217.
- [8] Keerthi, K.D., Santra, B.K., and Lahiri, G.K., 1998, Ruthenium(II) bipyridine complexes with modified phenolic Schiff base ligands. Synthesis, spectroscopic characterization and Redox properties, *Polyhedron*, 17 (8), 1387–1396.
- [9] Demetgül, C., Deletioğlu, D., Karaca, F., Yalçinkaya, S., Timur, M., and Serin, S., 2010, Synthesis and characterization of a Schiff base derived from 2-aminobenzylamine and its Cu (II) complex: Electropolymerization of the complex on a platinum electrode, *J. Coord. Chem.*, 63 (12), 2181–2191.
- [10] Makal, A., Schilf, W., Kamiński, B., Szady-Chelmieńska, A., Grech, E., and Woźniak, K., 2011, Hydrogen bonding in Schiff bases – NMR, structural and experimental charge density studies, *Dalton Trans.*, 40 (2), 421–430.
- [11] Gharagozlou, M., Baradaran, Z., and Bayati, R., 2015, A green chemical method for synthesis of ZnO nanoparticles from solid-state decomposition of Schiff-bases derived from amino acid alanine complexes, *Ceram. Int.*, 41 (7), 8382–8387.
- [12] Wang, Y.X., Shen, Z.C., Huang, D.D., and Yang, Z.S., 2018, High-performance ZnO nanosheets/nanocrystalline aggregates composite photoanode film in dye-sensitized solar cells, *Mater. Lett.*, 214, 88–90.
- [13] Meng, L., Xu, Q., Sun, Z., Li, G., Bai, S., Wang, Z., and Qin, Y., 2018, Enhancing the performance of room temperature ZnO microwire gas sensor through a combined technology of surface etching and UV illumination, *Mater. Lett.*, 212, 296–298.
- [14] Saleem, S., Jameel, M.H., Akhtar, N., Nazir, N., Ali, A., Zaman, A., Rehman, A., Butt, S., Sultana, F., Mushtaq, M., Zeng, J.H., Amami, M., and Althubeiti, K., 2022, Modification in structural, optical, morphological, and electrical properties of zinc oxide (ZnO) nanoparticles (NPs) by metal (Ni, Co) dopants for electronic device applications, *Arabian J. Chem.*, 15 (1), 103518.
- [15] Khalaji, A.D., 2019, Preparation and characterization of ZnO nanoparticles via thermal decomposition from zinc(II) Schiff base complex as new precursor, *Chem. Methodol.*, 3 (5), 571–579.
- [16] Li, Q., Cao, W., Lei, J., Zhao, X., Hou, T., Fan, B., Chen, D., Zhang, L., Wang, H., Xu, H., Zhang, R.,

- and Lu, H., 2014, Synthesis and growth mechanism of ZnO rod-like nanostructures by a microwave-assisted low-temperature aqueous solution route, *Cryst. Res. Technol.*, 49 (5), 298–302.
- [17] Zhang, X.L., Dai, H.T., Zhao, J.L., Wang, S.G., and Sun, X.W., 2014, Surface-morphology evolution of ZnO nanostructures grown by hydrothermal method, *Cryst. Res. Technol.*, 49 (4), 220–226.
- [18] Li, T., Cao, Z., You, H., Xu, M., Song, X., and Fang, J., 2013, Controllable growth of ZnO mesocrystals using a facile electrochemical approach, *Chem. Phys. Lett.*, 555, 154–158.
- [19] Salavati-Niasari, M., Gholami-Daghian, M., Esmaeili-Zare, M., and Sangsefidi, F.S., 2013, Solid state synthesis and characterization of zinc oxide (ZnO) microflakes by [bis(acetylacetonato)zinc(II)] and sodium hydroxide at room temperature, *J. Cluster Sci.*, 24 (4), 1093–1101.
- [20] Galini, M., Salehi, M., Kubicki, M., Bayat, M., and Malekshah, R.E., 2020, Synthesis, structural characterization, DFT and molecular simulation study of new zinc-Schiff base complex and its application as a precursor for preparation of ZnO nanoparticle, *J. Mol. Struct.*, 1207, 127715.
- [21] Shahraki, S., and Heydari, A., 2017, New zinc(II) N4 tetradentate Schiff base complex: A potential cytotoxic metallodrug and simple precursor for the preparation of ZnO nanoparticles, *Colloids Surf., B*, 160, 564–571.
- [22] Ortigón-Reyna, D., Garcías-Morales, C., Padilla-Martínez, I., García-Báez, E., Aríza-Castolo, A., Peraza-Campos, A., and Martínez-Martínez, F., 2013, NMR structural study of the prototropic equilibrium in solution of Schiff bases as model compounds, *Molecules*, 19 (1), 459–481.
- [23] Vaz, P.A.A.M., Rocha, J., Silva, A.M.S., and Guieu, S., 2018, Aggregation-induced emission enhancement of chiral boranils, *New J. Chem.*, 42 (22), 18166–18171.
- [24] Alothman, A.A., and Albaqami, M.D., 2020, Nano-sized Cu(II) and Zn(II) complexes and their use as a precursor for synthesis of CuO and ZnO nanoparticles: A study on their sonochemical synthesis, characterization, and DNA-binding/cleavage, anticancer, and antimicrobial activities, *Appl. Organomet. Chem.*, 34 (10), e5827.
- [25] Silverstein, R.M., and Bassler, G.C., 1962, Spectrometric identification of organic compounds, *J. Chem. Educ.*, 39 (11), 546.
- [26] Bader, A.T., Al-qasii, N.A.R., Shntaif, A.H., El Marouani, M., AL Majidi, M.I.H., Trif, L., and Boulhaoua, M., 2022, Synthesis, structural analysis and thermal behavior of new 1,2,4-triazole derivative and its transition metal complexes, *Indones. J. Chem.*, 22 (1), 223–232.
- [27] Katouah, H.A., 2021, Facile synthesis of Co<sub>3</sub>O<sub>4</sub> and ZnO nanoparticles by thermal decomposition of novel Co(II) and Zn(II) Schiff base complexes for studying their biological properties and photocatalytic degradation of crystal violet dye, *J. Mol. Struct.*, 1241, 130676.
- [28] Muthukumar, S., and Gopalakrishnan, R., 2012, Structural, FTIR and photoluminescence studies of Cu doped ZnO nanopowders by co-precipitation method, *Opt. Mater.*, 34 (11), 1946–1953.
- [29] Viezbicke, B.D., Patel, S., Davis, B.E., and Birnie III, D.P., 2015, Evaluation of the Tauc method for optical absorption edge determination: ZnO thin films as a model system, *Phys. Status Solidi B*, 252 (8), 1700–1710.
- [30] Talam, S., Karumuri, S.R., and Gunnam, N., 2012, Synthesis, characterization, and spectroscopic properties of ZnO nanoparticles, *Int. Scholarly Res. Not.*, 2012, 372505.
- [31] Sales Amalraj, A., Christina Joyce, S., and Natarajan, G., 2022, Investigation of the properties of tungsten doped ZnO thin films synthesised by SILAR method, *Mater. Res. Innovations*, 26 (5), 263–269.
- [32] Doustkhah, E., Esmat, M., Fukata, N., Ide, Y., Hanaor, D.A.H., and Assadi, M.H.N., 2022, MOF-derived nanocrystalline ZnO with controlled orientation and photocatalytic activity, *Chemosphere*, 303, 134932.
- [33] Kinra, S., Ghosh, M.P., Mohanty, S., Choubey, R.K., and Mukherjee, S., 2022, Manganese ions

- substituted ZnO nanoparticles: Synthesis, microstructural and optical properties, *Phys. B*, 627, 413523.
- [34] Sa'aedi, A., Akl, A.A., and Hassanien, A.S., 2022, Effective role of Rb doping in controlling crystallization, crystal imperfections, microstructural, and morphological features of ZnO-NPs synthesized by sol-gel approach, *CrystEngComm*, 24 (26), 4661–4678.
- [35] Geetha, M.S., Nagabhushana, H., and Shivananjaiiah, H.N., 2016, Green mediated synthesis and characterization of ZnO nanoparticles using *Euphorbia Jatropa* latex as reducing agent, *J. Sci.: Adv. Mater. Devices*, 1 (3), 301–310.
- [36] Jin, S.E., Hwang, S.J., and Jin, H.E., 2022, Hierarchical tetramodal-porous architecture of zinc oxide nanoparticles microfluidically synthesized via dual-step nanofabrication, *Mater. Des.*, 215, 110486.